CGMS-34, NOAA-WP-14
Prepared by M. Goldberg
Agenda Item: II/4
Discussed in WG2

2005 / 2006 Report on NOAA/NESDIS Satellite-Derived Winds

NOAA-WP-14 summarizes the current NOAA/NESDIS operational wind product suite that includes the high density cloud-drift winds from the GOES imager, water vapor motion winds derived from the GOES sounder, and cloud-drift and water vapor winds from the MODIS instrument aboard NASA's Terra and Aqua satellites. Research and development activities involving new satellite-derived wind products and improvements to existing satellite-derived wind products are also summarized.

2005/2006 REPORT ON NOAA/NESDIS SATELLITE-DERIVED WINDS

Jaime Daniels[1], Chris Velden [2], Jeff Key[1], Wayne Bresky[3], David Santek[2], W. Paul Menzel[1],
Mitch Goldberg[1]

[1] - NOAA/NESDIS/STAR

[2] - Cooperative Institute for Meteorological Satellite Studies
Madison, Wisconsin

[3] – Raytheon Information Solutions
Lanham, Maryland

1. Introduction

NOAA/NESDIS and the Cooperative Institute for Meteorological Satellite Studies (CIMSS) continue collaborations aimed at improving the quality of Atmospheric Motion Vectors (AMVs) derived from NOAA's Polar and Geostationary Operational Environmental Satellites as well as from NASA's Terra and Aqua polar orbiting satellites. NOAA/NESDIS continues to generate a large suite of AMV products from these satellites on an operational basis. A description of these products and their quality is described in Section 2. Section 3 describes the active satellite AMV research that took place over the past year. This research occurred in a number of areas that includes: characterization of height assignment errors, AMV quality control, the derivation and application of AMVs from rapid scan GOES imagery, development of a new approach to improving GOES navigation and assessing its impact on AMV quality, investigating optical flow approaches to the problem of feature tracking, and the development of techniques to generate AMVs from the Advanced Very High Resolution Radiometer (AVHRR) imagery.

2. Status and Performance of Operational Wind Products

The operational AMV products currently being generated at NOAA/NESDIS are shown in Table 1. The frequency at which each product is produced, together with the GOES image sector used, and image interval is presented in this table. All of the AMV products shown in this table are encoded into the World Meteorological Organization (WMO)-sanctioned Binary Universal Form for the Representation (BUFR) of meteorological data and distributed over the Global Telecommunication System (GTS). The last column of the table lists the WMO headers used to uniquely identify each of these NESDIS AMV products. All of the products, with the exception of the sounder water vapor winds, will continue to be encoded into the SATOB format and distributed over the Global Telecommunication System (GTS).

During the period 2005-2006, some changes to the operational NOAA/NESDIS processing environment took place. Starting on 21 June 2006, GOES-11 replaced GOES-10 as the western operational geostationary satellite. AMVs generated from GOES-11 are very similar to those generated from GOES-10 since the spectral coverage and resolution of the GOES-11 imager and sounder instruments are very similar to the spectral coverage and resolution of the GOES-10 image and sounder instruments. On 17 March 2006, NOAA/NESDIS ceased production of the low-level "picture-triplet" cloud-drift wind products. Beginning on 19 September 2006, NOAA/NESDIS began distributing the Terra and Aqua MODIS AMVs over the GTS. This distribution path gave operational Numerical Weather Prediction (NWP) centers easy access to these AMV products.

In the near future, NOAA/NESDIS will begin testing the generation of AMVs on an hourly basis instead of a three hourly basis. In anticipation of establishing this capability, a computer system architecture change was made within NOAA/NESDIS' computing environment for the production of GOES and

MODIS AMVs. SGI workstations, running the IRIX operating system, were replaced by Dell servers, running the LINUX Redhat operating system. The operational AMV product processing software was successfully ported and tested within this new architecture. Reduced AMV product latency times, of up to 40%, are observed as a result of the faster processors. With this new computing architecture now successfully in place, experimental production and distribution of hourly GOES AMV products can be done. Present plans call for experimental production and distribution of hourly GOES AMV product files in BUFR in November 2006. The AMV user community will be notified when these files are made available.

Like other satellite producers, NOAA/NESDIS continues to rely on collocated AMVs and rawinsonde observations to assess and monitor the quality the AMVs. Time series of verification statistics can be found at: http://www.orbit.nesdis.noaa.gov/smcd/opdb/goes/winds/html/tseries.html.
Figure 1 (top) shows time series of daily (at 00Z and 12Z) verification statistics (satellite-rawinsonde mean vector difference and wind speed bias) for upper level (100-400mb) GOES-12 LWIR cloud- drift winds and water vapor winds in the Northern and Southern Hemispheres for the period 02 September 2005 – 19 September 2006. Figure 1 (bottom) shows a time series of verification statistics for low level (700-100mb) GOES-12 LWIR and visible cloud-drift winds for the same time period. Similarly, the verification statistics for GOES-10 for the period 01 September 2005 – 21 June 2006 are shown in Figure 2.

Wind Product	*Frequency (Hours)*	*Image Sector(s)*	*Image Interval (minutes)*	*GTS WMO Header*
GOES IMAGER				
LWIR (11um) Cloud-drift	3	RISOP	7.5	JACX11- GOES-E JCCX11- GOES-W
	3	CONUS	15	
	3	Extended NH: SH	30	
SWIR (3.9um) Cloud-drift	3 (Night-time)	RISOP	7.5	JQCX11- GOES-E JRCX11- GOES-W
	3 (Night-time)	CONUS	15	
	3 (Night-time)	Extended NH: SH	30	
Water Vapor (6.7um)	3	Extended NH; SH	30	JECX11- GOES-E JGCX11- GOES-W
Vis Cloud-drift (0.65um)	3 (Daytime)	RISOP	7.5	JHCX11- GOES-E JJCX11- GOES-W
	3 (Daytime)	PACU/CONUS	15	
	3 (Daytime)	Extended NH; SH	30	
GOES SOUNDER				
Sounder WV (7.4um)	3,6	CONUS/Tropical	60	JKCX11- GOES-E JMCX11- GOES-W
Sounder WV (7.0um)	3,6	CONUS/Tropical	60	JNCX11- GOES-E JPCX11- GOES-W
TERRA/AQUA MODIS				
LWIR (11um) Cloud-drift	2	NH; SH (Poleward of 65° Lat)	100	JBCX11- Terra JICX11 - Aqua
Water Vapor (6.7um)	2	NH; SH (Poleward of 65° Lat)	100	JFCX11- Terra JILX11 - Aqua

Table 1. **GOES Imager/Sounder and Terra/Aqua MODIS atmospheric motion vector products generated by NOAA/NESDIS**

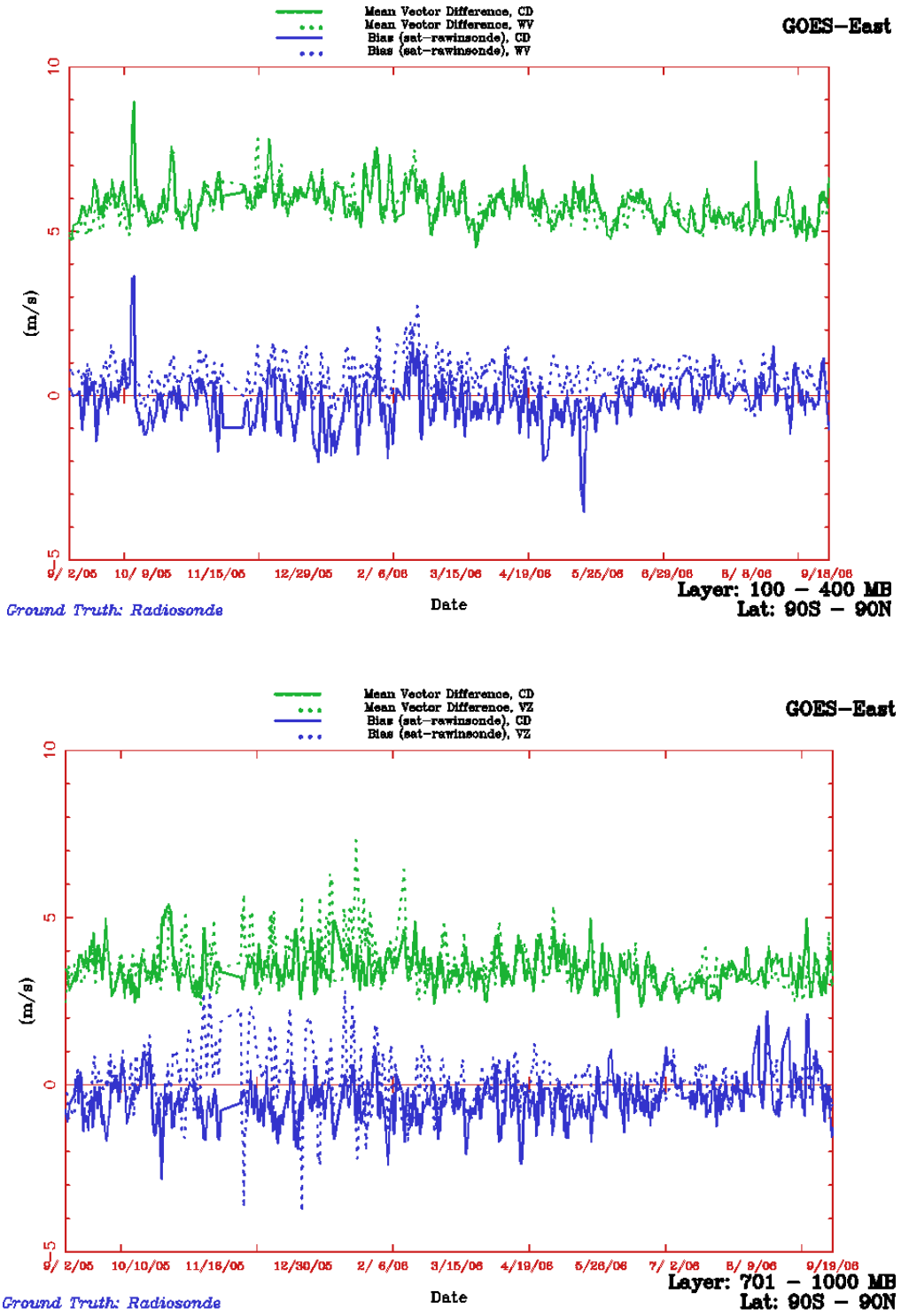

Figure 1. **Mean vector difference and speed bias (sat-rawinsonde) for GOES-12 upper level (100-400mb) LWIR cloud-drift and WV winds** (top) **and lower level (700-1000mb) LWIR and Visible cloud-drift winds** (bottom)**.**

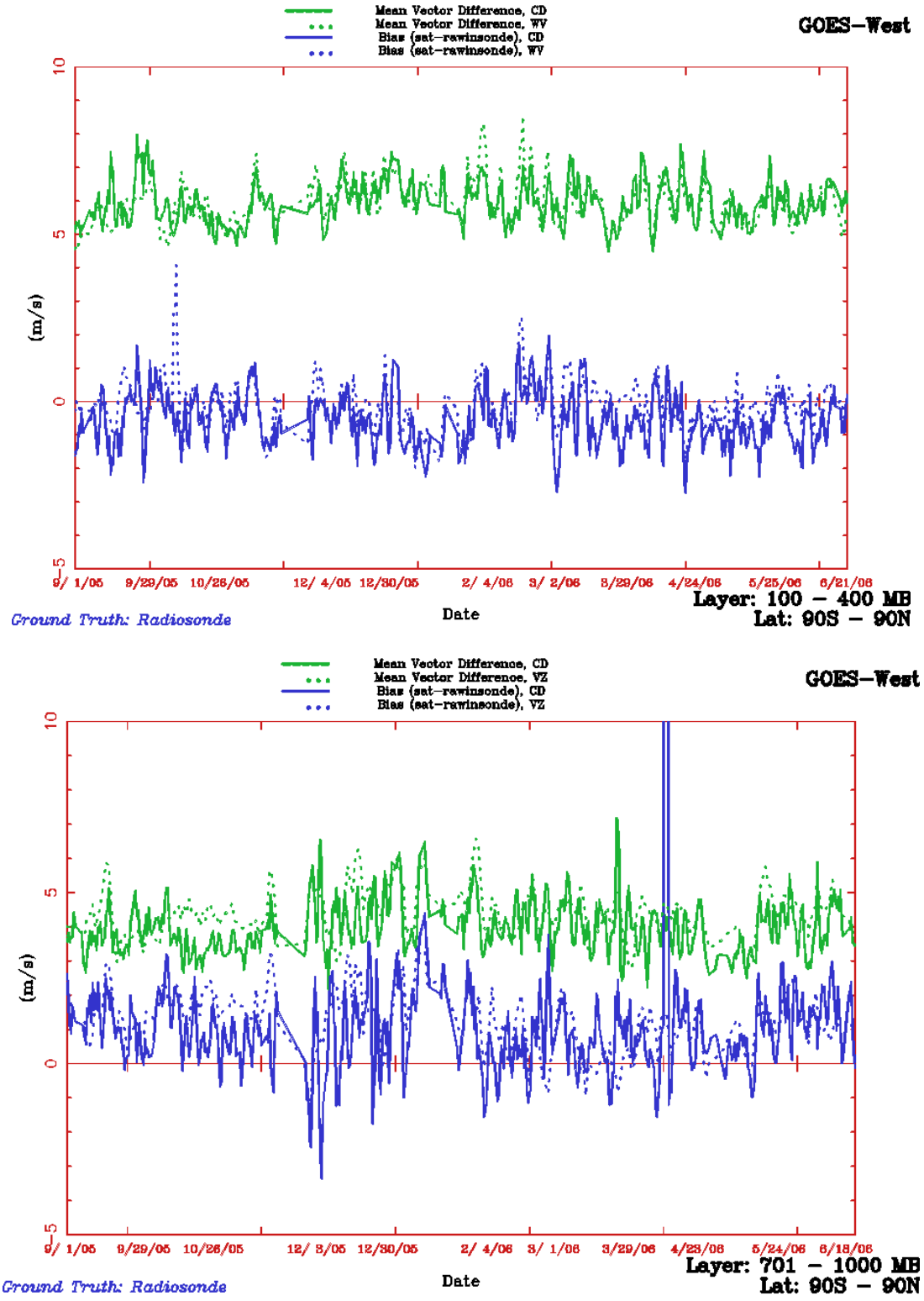

Figure 2. Mean vector difference and speed bias (sat-rawinsonde) for GOES-10 upper level (100-400mb) LWIR cloud-drift and WV winds **(top)** and lower level (700-1000mb) LWIR and Visible cloud-drift winds **(bottom)**.

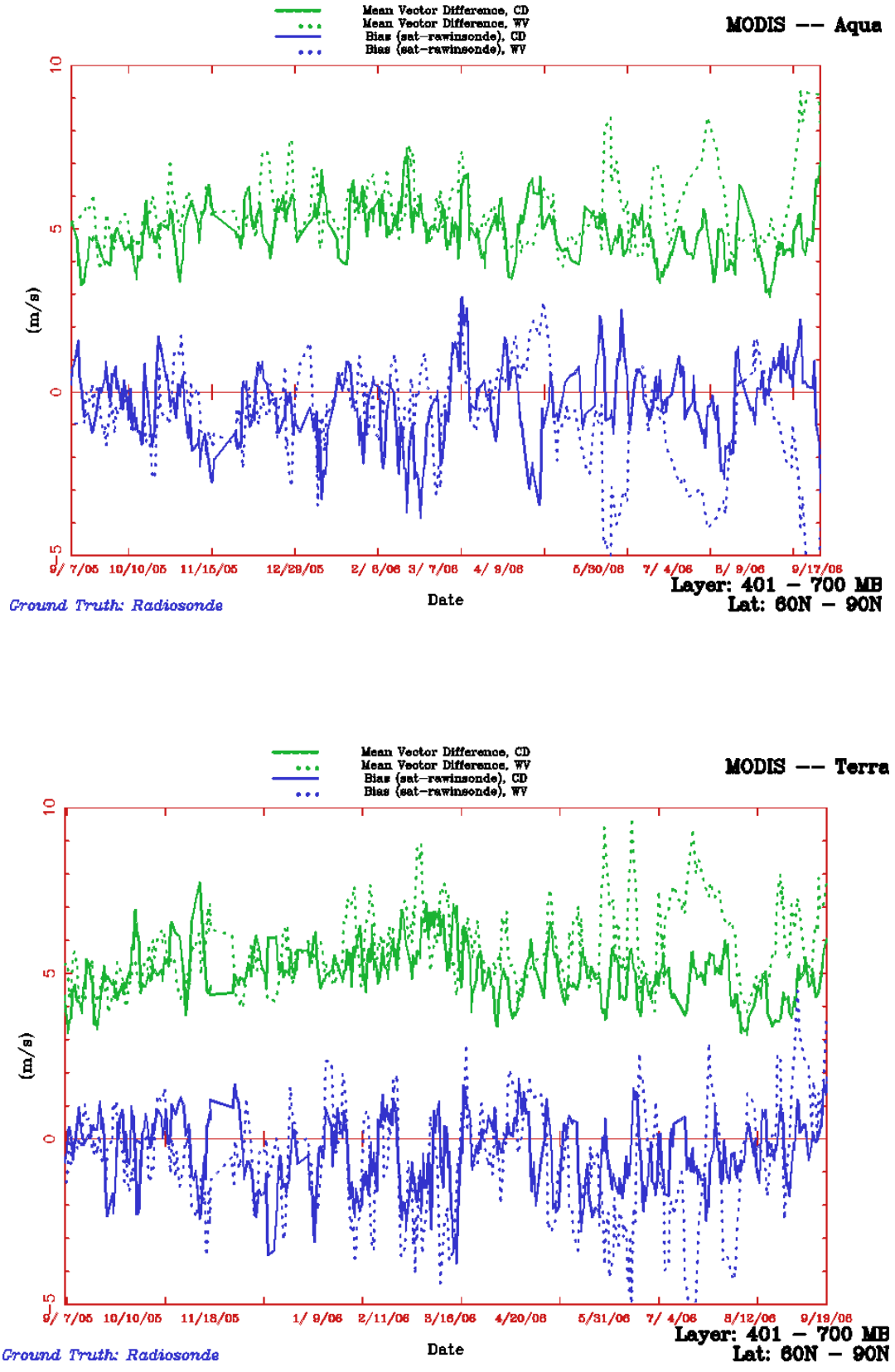

Figure 3. Mean vector difference and speed bias (sat-rawinsonde) for NHEM Aqua MODIS mid level (400-700mb) LWIR cloud-drift and WV winds (top) and NHEM Terra mid level (400-700mb) LWIR and WV winds (bottom).

Like the GOES AMV products, the quality of the Terra and Aqua MODIS AMV products are monitored via comparisons with collocated rawinsonde observations. While the number of rawinsondes observations in the Arctic and Antarctic regions is limited, the comparison statistics that are generated still provide useful information on the quality of the MODIS AMVs. Figure 3 (top) shows time series of daily (at 00Z and 12Z) verification statistics (satellite-rawinsonde mean vector difference and wind speed bias) for mid level (400-700mb) Aqua LWIR cloud-drift winds and water vapor winds in the Northern Hemisphere for the period 07 September 2005 – 17 September 2006. Figure 2 (bottom) shows the time series of verification statistics but for mid-level (400-700mb) Terra LWIR cloud-drift winds and water vapor winds in the Northern Hemisphere. The verification statistics for Southern Hemisphere Aqua and Terra MODIS AMVs, while not shown, show similar results.

3. Research and Development Activities

3.1 Polar Winds from MODerate Resolution Imaging Spectroradiometer (MODIS) Data

Use of MODIS Winds in Operational Forecast Systems

Given the sparsity of wind observations in the polar regions, satellite-derived polar wind information has the potential to improve forecasts in polar and sub-polar areas. Nine numerical weather prediction (NWP) centers have performed model impact studies and found that, overall, the impact of the MODIS polar winds is positive. Most centers have demonstrated a positive impact in the Arctic and Antarctic as well as the extratropics of both hemispheres, though the magnitude of the impact varies among the centers. The following NWP centers that are currently assimilating the MODIS winds in their operational forecast systems include:

- European Center for Medium-Range Weather Forecasts (ECMWF)
- NASA Global Modeling and Assimilation Office (GMAO)
- (UK) Met Office
- Canadian Meteorological Centre (CMC)
- Japan Meteorological Agency (JMA)
- US Navy, Fleet Numerical Meteorology and Oceanography Center (FNMOC)
- National Centers for Environmental Prediction (NCEP)
- Deutscher Wetterdienst (DWD)
- MeteoFrance

Combined Terra and Aqua MODIS

Operationally at NESDIS, winds from the Terra and Aqua satellites are generated separately. Some improvements in wind quality and timeliness could be obtained by combining imagery from the two satellites into the same processing stream. Utilizing the combined Terra/Aqua MODIS data stream will require that imagery be corrected for parallax, as the two satellites will view the same cloud or water vapor features from different angles. Without a parallax correction, errors in location, and therefore wind speed and direction, can be significant. Routine, but experimental, wind processing using the combined data stream has been implemented. The results are under evaluation.

Direct Broadcast MODIS Winds

The MODIS polar winds product typically lags the observing time (the time MODIS views an area) by 3-5 hours. The lag is largely due to the delay in the availability of the level 1B MODIS data, which are acquired through a NOAA computer system at the NASA Goddard Space Flight Center. The lag also includes a delay of 100 minutes because three consecutive orbits are used to derive the winds, and the final time is assigned that of the middle orbit. The 3-5 hour delay is too long for the early runs of most data assimilation systems. It may be possible to reduce the delay by obtaining data from direct broadcast (DB) sites, with the added benefit of providing local forecasters with real-time wind information.

A system to generate the MODIS winds with direct broadcast MODIS data has been developed and implemented at McMurdo, Antarctica, using an antenna purchased by the U.S. National Science Foundation. MODIS wind production at McMurdo began in April 2005. Figure 4 gives an example of the direct broadcast polar winds over Antarctica. A similar system was installed at Tromsø, Norway, using an antenna on Svalbard. Routine wind production at Tromsø began in March 2006 (Terra only). Winds can be generated with a delay on the order of 2 hours (again, including the offset time for middle image targeting) rather than 3-5 hours. Similar MODIS winds systems will be installed at direct broadcast sites in Finland and Alaska within the next year. Real-time results for McMurdo and Tromsø are available at http://stratus.ssec.wisc.edu/products/db/.

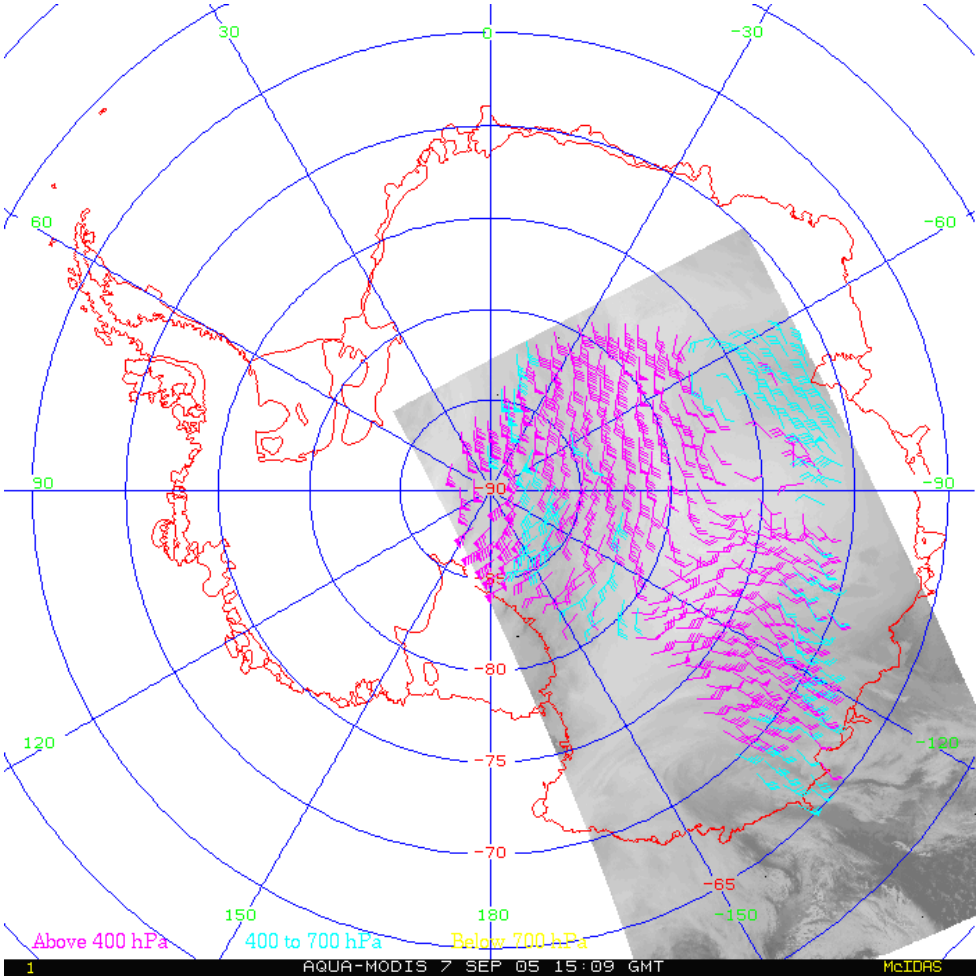

Figure 4. **Winds generated from direct broadcast Aqua MODIS data obtained at McMurdo, Antarctica, on 7 September 2005.**

3.2 Polar Winds from Advanced Very High Resolution Radiometer (AVHRR) Data

With the continuing availability of AVHRR on NOAA satellites and Metop, and as the MODIS instruments move toward (or beyond) their life expectancies, there is an increasing interest in polar winds from AVHRR. The MODIS winds processing system has recently been adapted for use with the AVHRR, and winds from NOAA-15, -16, -17, and -18 are being generated experimentally in near real-time (http://stratus.ssec.wisc.edu/products/rtpolarwinds). Validation of the AVHRR winds is in progress. An example is shown in Figure 5.

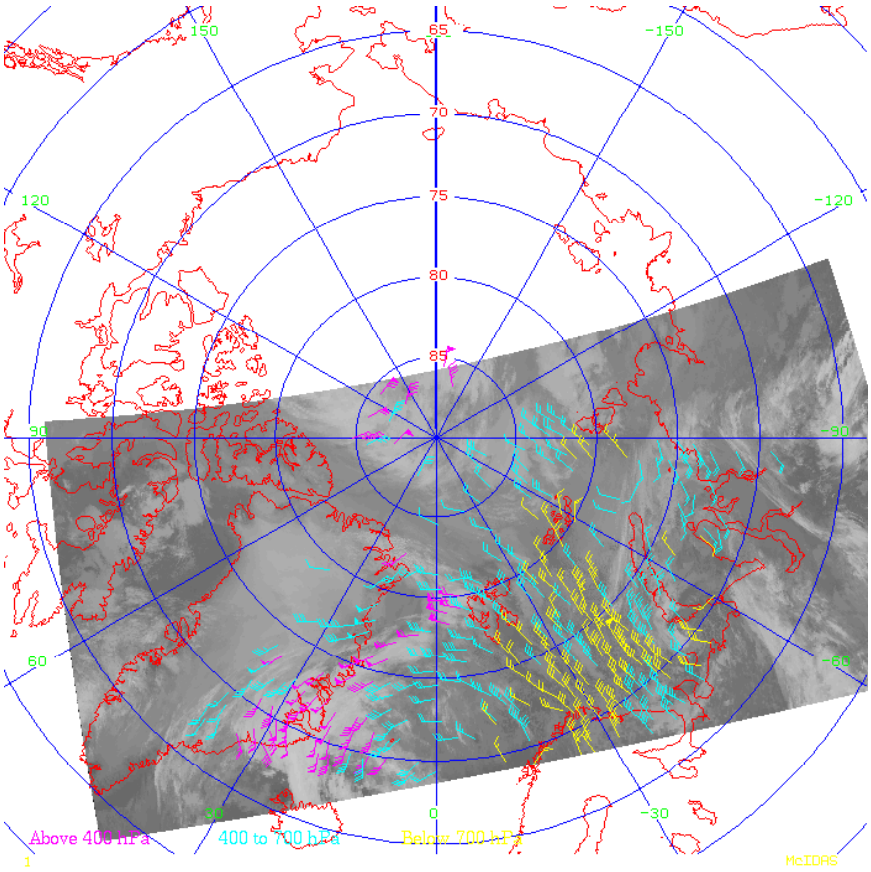

Figure 5. **Winds generated from NOAA-17 AVHRR on 15 September 2006 over the Arctic**.

3.3 New Expected Error Quality Indicator Applied to GOES and MODIS AMVs

The Expected Error (EE) quality control approach developed at the Australian Bureau of Meteorology (LeMarshall et al, 2004), has been successfully tested for GOES and MODIS at the Joint Center for Satellite Assimilation (JCSDA), NOAA/NESDIS/STAR, and at CIMSS. This method extends and modifies the current AMV quality indicator (QI) scheme that is used operationally by numerical forecast centers to thin the AMV input. The new algorithm linearly regresses several AMV parameters against co-located RAOBS. Coefficients from the regressions can then be used to come up with "expected errors" (EE) for each derived vector.

The expected error was created, in part, to improve the relationship between a given quality indicator and the AMV – RAOB difference. Thus, it is worth comparing the skill of the expected error as compared to the QI: the indicator the expected error is enhancing. Figure 6 shows RMS statistics of AMV – RAOB differences of winds as binned by a central expected error value (red circled curve) and a central QI (blue x curve). In other words, an expected error bin of 5 ms^{-1} corresponds to winds that have expected errors between 4.5 and 5.5. The rms of the AMV - RAOB differences for those winds are what is plotted in the figure. The numbers on each curve represent the number of winds in each bin. The four plots correspond to winds produced from different channels: NHIR (upper-left), NHVS (upper-right), NHWV (lower-left) and NHSWIR (lower-right). The dashed-line on each of the plots represents a 1-1 line. If the expected error were a perfect predictor of the actual error, each of the points would fall on this line.

As the plots show, however, although the expected error is often close to this line, it varies by about a meter per second from this line at various points. The actual error also shows sensitivity to the QI (corresponding to the top axis). As the QI increases, the actual error decreases slightly, but at a less rapid rate than for the expected error. In general, the range of actual error values is larger for the expected error ranges shown than for the QI ranges shown corresponding to a stronger sensitivity.

These results imply that the expected error is a better predictor of wind quality than the corresponding QIs.

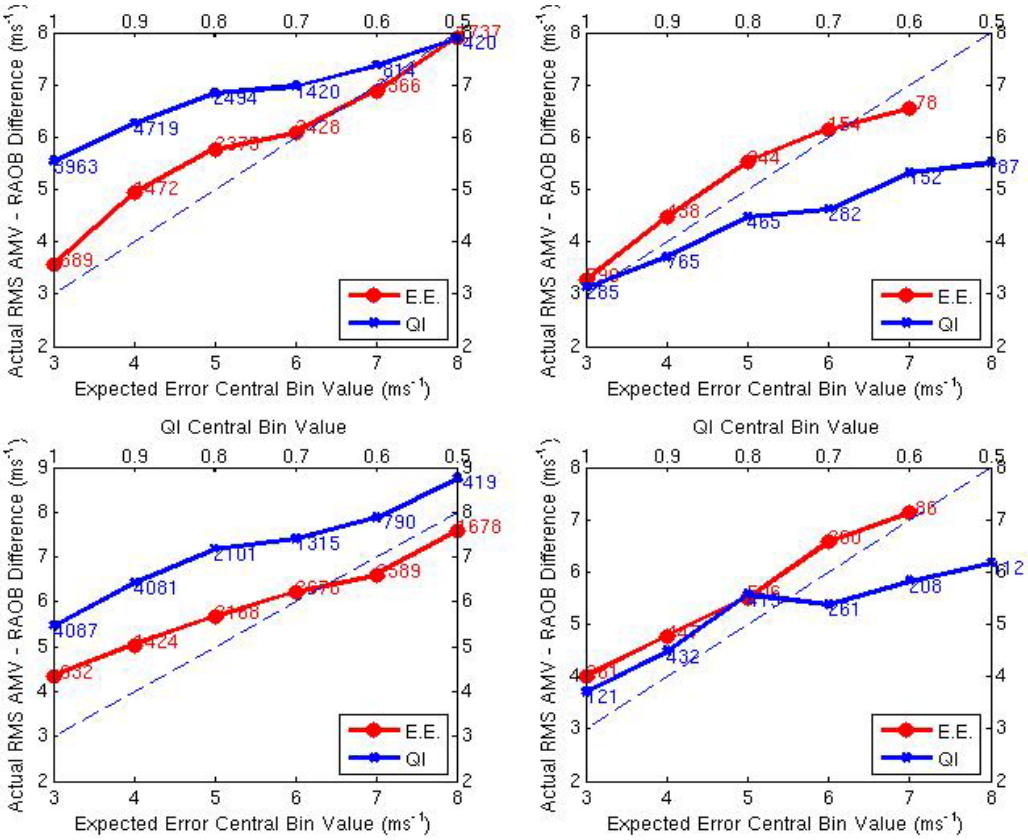

1

Figure 6. **Comparisons of expected error bins (red circles) and QI bins (blue x's) as a measure of the RMS of the actual AMV – RAOB difference for NHIR (upper-left), NHVS (upper-right), NHWV (lower left) and NHSWIR (lower – right). The lower axis corresponds to expected error and the upper axis corresponds to the QI. The number of matches in each bin is also shown. In general, the expected error shows a stronger relationship with the actual error as compared to RAOBS for each channel.**

The expected error has shown to be a reasonable measure of the difference between AMVs and RAOBS. Keep in mind that it is not a true measure of the observation error. The observation error, in a data assimilation context, is defined as the difference between an observation and the truth. Expected error also includes RAOB error and representative error between the AMV and the RAOB. Also, the expected error has been calculated after the AMV quality control has been applied. As a result, most of the bad winds have already been rejected. Finally, the expected error naturally increases with wind speed. Attempts to normalize expected error by the wind speed did not add value to the indicator. Even with these contingencies, the expected error has shown skill in demonstrating the quality of AMVs.

At the present time, the EE quality control approach has been successfully implemented within the operational winds processing system at NOAA/NESDIS. The EE quality flag has been added to the AMV BUFR template and experimental AMV BUFR files are being routinely made available to the NWP community for model impact assessments. The addition of this new AMV quality flag, together with the AMV quality flags that already exist in the BUFR template, are expected to allow NWP users to improve their ability to preferentially select the highest quality AMVs that will be used in their operational data assimilation schemes.

3.4 Winds from Rapid-Scan Imagery

In the United States, GOES has been used in operational forecasting for quite some time. Forecasters recognize the additional detail that can be captured from more frequent imaging in events associated with rapidly changing cloud structures. The value of more frequent imaging is evidenced by the inclusion of a 15-minute update cycle over the Continental United States (CONUS) sector in the current GOES schedule, and by the multitude of special National Weather Service (NWS) operational requests for more frequent sampling at 7.5 minute intervals (Rapid-Scan OPerations, RISOP). On occasion, special periods of Super-Rapid-Scan Operations (SRSO) have been requested by the research community. The SRSO allow limited-area coverage of one-minute interval sampling over meteorological events of interest.

Recently, special GOES RISOP periods have been collected during several field programs and research initiatives designed to maximize observational abilities in regions of high-impact weather events. Some examples include the NASA Tropical Cloud Systems Program (TCSP) in 2005, and the TROpical Predictability EXperiment (TROPEX) in 2005/2006. In the TCSP, the AMV datasets were used in real time in mission planning and/or directing aircraft to targets of opportunity. In TROPEX, the AMV datasets are being used in targeted observing strategy experiments run by modelers at the Naval Research Laboratory. Initial results, shown in Figures 7 and 8, are quite promising and indicate that GOES rapid scan winds are valuable observations in areas deemed sensitive and in need of more observations for the successful forecasting of downstream high impact weather events.

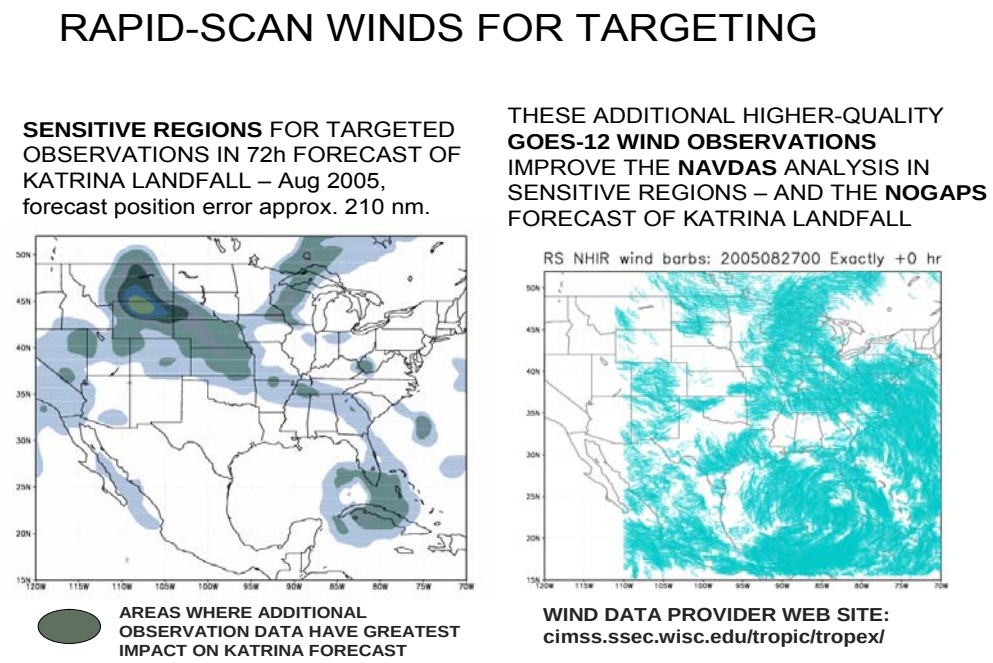

Figure 7. **NRL-MRY targeting experiments with GOES rapid-scan AMVs.**

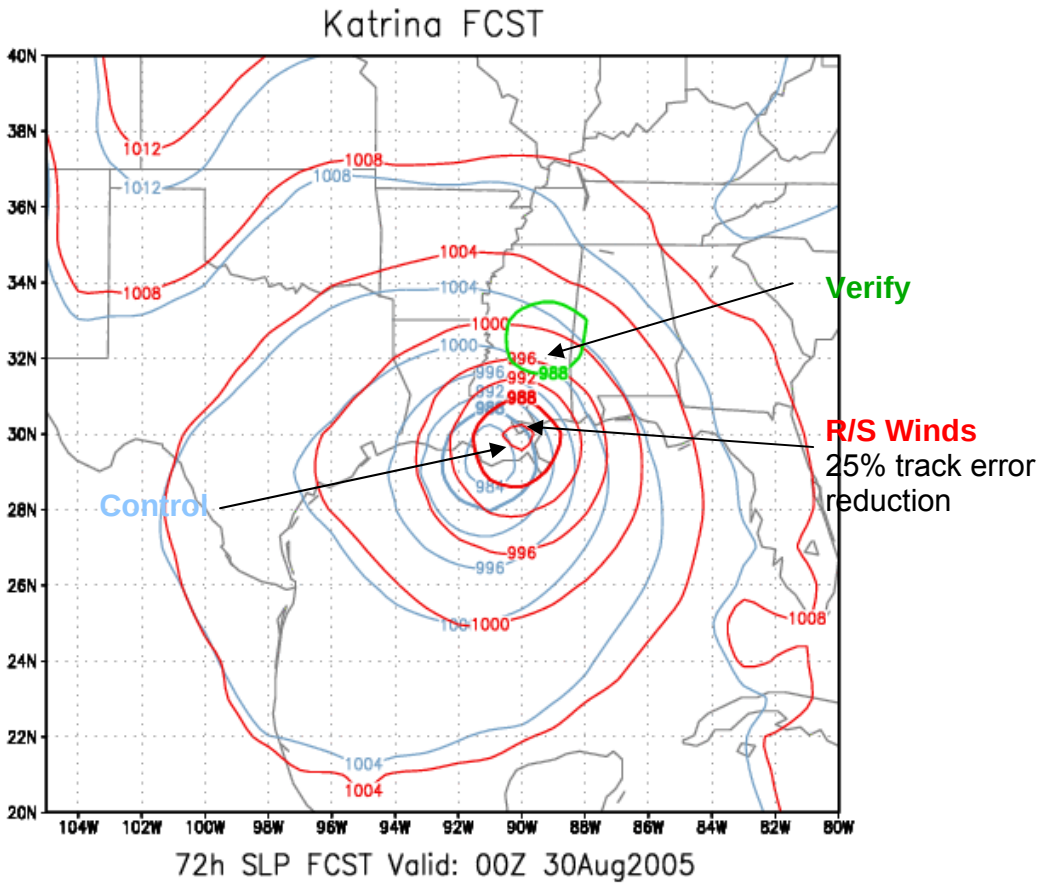

Figure 8. **Example of positive impact of GOES-12 rapid scan AMVS on NWP forecast of Hurricane Katrina.**

3.5 Investigation of Optical Flow Approaches

In the computer vision field, optical flow is one of the standard techniques in computing motion vectors from two subsequent images (Sonka et al, 1993; Barron et al, 1994). Optical flow is defined as the apparent motion of image brightness patterns in an image sequence. Recent research performed at NOAA/NESDIS has focused on the application of optical flow techniques to derive AMV products. The optical flow algorithm tested at NOAA/NESDIS is described in Lucas and Kanade, 1981. Two underlying assumptions in this approach are that local changes in intensity are explained only by motion and that the motion is uniform over a small area. Implementation of this approach involves a sequence of five images which are smoothed in both the spatial and temporal domains using a Gaussian filter. The target selection algorithm used is the one used operationally at NOAA/NESDIS. This was done to facilitate the comparison of the test winds with the control winds. The performance this optical flow algorithm was then evaluated against the performance of the traditional pattern matching technique (sum of squared differences) being used operationally at NOAA/NESDIS.

The algorithm was tested initially on an image sequence with a controlled displacement to validate the results and measure the algorithm's performance. The optical flow algorithm outlined above was tested initially on a sequence of images with a known displacement. The starting point for the sequence was a single, full resolution, GOES-11 infrared image. This initial image was displaced by a known amount (2-lines south; 2 elements east) a total of four times to produce a sequence of five images, all exhibiting the same shift. The entire sequence was smoothed spatially and temporally. A similar, but un-smoothed, test sequence was also created for the purpose of generating winds with the

routine, correlation-based, algorithm. The results achieved with the test sequence are shown in Figure 9 and indicate that the optical flow algorithm

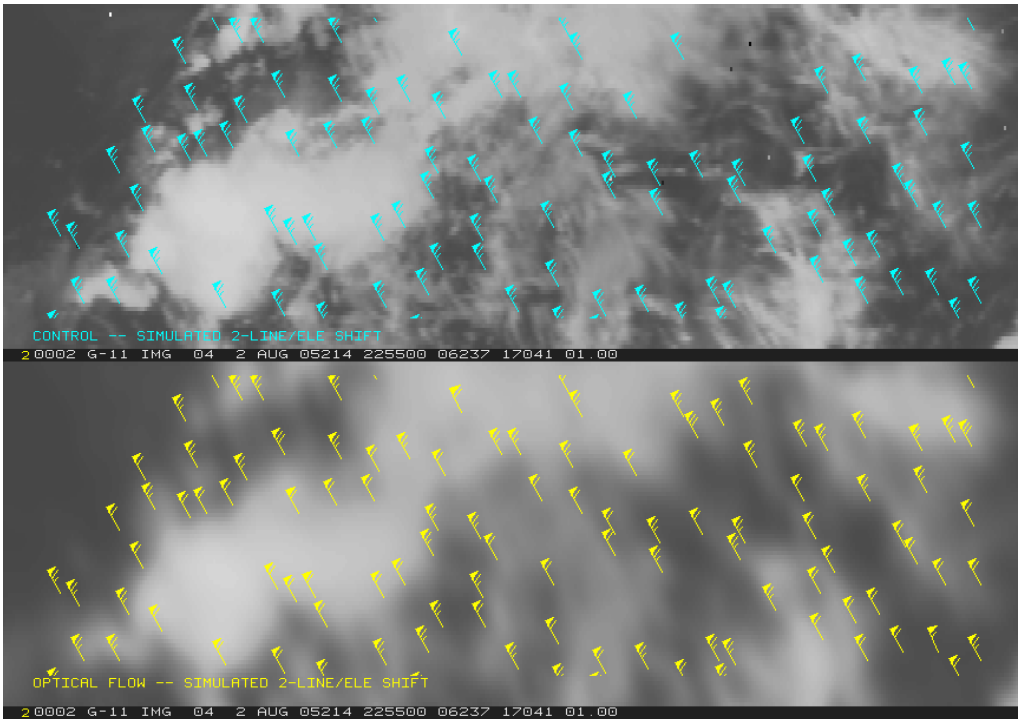

Figure 9. **The control (top) and optical flow (bottom) winds generated using a test sequence with a known displacement (2-lines/elements).**

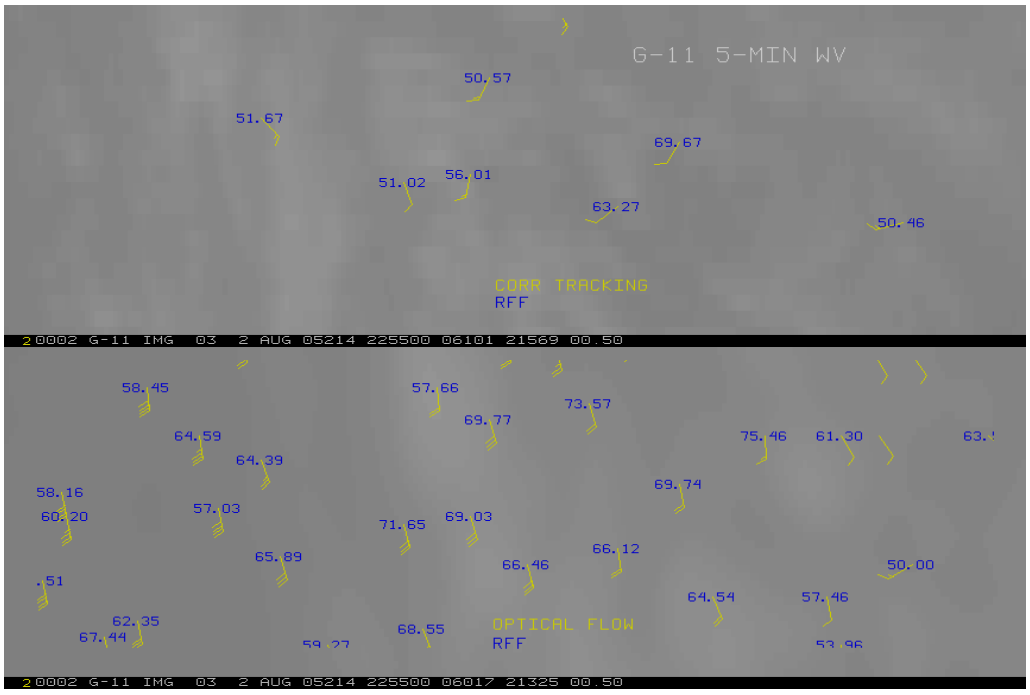

Figure 10. **The routine (top) and optical flow (bottom) winds for 2255Z August 2, 2005. The recursive filter flag (RFF) value, an objective measure of quality, is shown in blue.**

works as intended while yielding results comparable to the correlation-based tracking method.

Following this initial testing, the optical flow approach was applied to an actual 5-minute GOES-11 water vapor sequence. Figure 10 shows the resulting AMVs of the optical flow approach (bottom) as compared to the AMVs using the traditional correlation-based tracking over a zoomed in portion of the domain. In this region of relatively low contrast, the optical flow method clearly outperforms the routine tracking method, as evidenced by the higher RFF (an objective measure of quality based on an analysis of forecast and satellite data) values in the bottom panel. Note also the much better coverage provided by the optical flow method. When the optical flow method was applied to GOES-12 rapid scan (7.5 min interval imagery) water vapor in a "quasi- routine" mode, the results were very encouraging. Table 2 shows comparison statistics of the GOES-12 clear-sky water vapor winds, generated using the optical flow algorithm and the traditional correlation based algorithm, against rawinsondes over the continental United States at 00 UTC on 04 April 2006. These statistics strongly suggest that the optical flow method is superior to the traditional correlation-based method for tracking clear-sky water vapor features.

Statistic	Correlation	Optical Flow
Mean Vector Difference	7.15	6.19
Normalized RMS	0.36	0.33
Sat-Raob Speed Bias	1.78	-0.57
Speed	23.82	20.85
Sample Size	160	160

Table 2. **Comparison statistics between collocated GOES-12 edited water vapor winds (clear sky) generated using correlation matching and optical flow tracking and rawinsondes at 00 UTC on 04 April 2006.**

Other findings from this research (not shown), indicate that the optical flow algorithm described here should not be used in jet regions, nor should it be used in its current form, to track convective clouds. In the former situation the feature of interest is likely to move beyond the boundary of the neighborhood, leading to an unreliable estimate. In the latter situation the brightness constancy assumption will clearly be violated. Given the relatively low (by computer vision standards) temporal resolution of today's operational satellites, the optical flow approach should probably be viewed as a replacement to correlation tracking only in certain limited situations. The initial results from the optical flow algorithm are encouraging, but more research is needed and planned.

3.6 Characterization of AMV Height Assignment

Level of Best-Fit Analysis

A Level of Best-Fit (LBF) analysis using collocated operational GOES-12 AMVs, NOAA wind profiler observations, and radiosonde wind observations was done in order to better understand and quantify the height assignment characteristics of the GOES-12 AMVs. Figure 11 shows the results of the LBF analysis involving collocated operational GOES-12 IR cloud-drift AMVs and rawinsondes over the one year period Jan 2004 to Jan 2005. The analysis results were stratified by the various height assignment methods applied to GOES-12 IR cloud-drift AMVs. LBF results at 200hPa, 300hPa, and 500hPa for the CO_2 slicing, H_2O-intercept, IRW height assignments are shown in this figure. The solid green curve is the vector RMS vector profile, the dashed green line is the speed bias (AMV-rawinsonde) profile, and the red line is the mean rawinsonde speed profile. The results indicate that, in general, reasonably accurate height assignments are given to the GOES-12 AMVs. However, the results also indicate that there is a strong tendency to assign GOES-12 AMVs too high up in the atmosphere, regardless of what height assignment method is used. This suggests the need to interrogate every aspect of the height assignment methodology used at NOAA/NESDIS. While not

shown here, further analysis and results indicate the need to apply a radiance bias correction to the 11um and 13.3um channels in order to improve the GOES-12 CO2 height assignments.

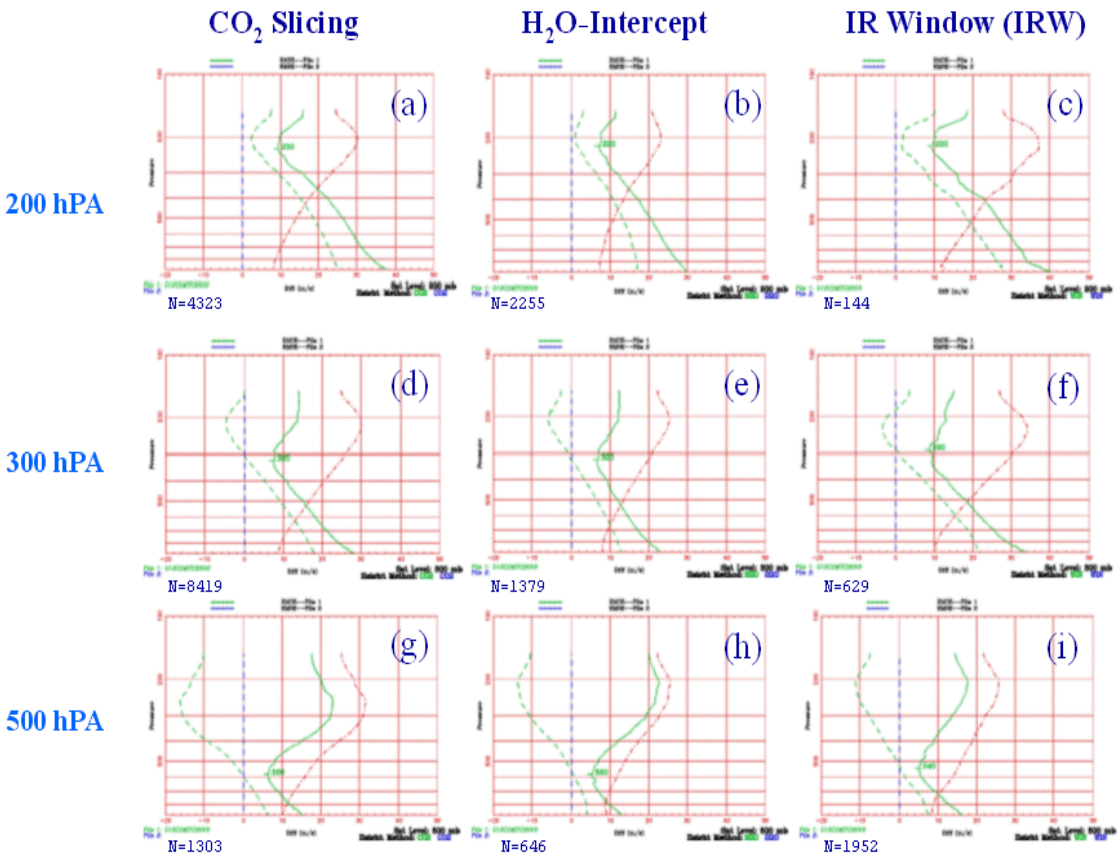

Figure 11. **Vertical vector RMS profiles between GOES-12 AMVs (at 200, 300, and 500 hPa) and collocated rawinsonde observations for different height assignment methods. Solid green curve is the vector RMS profile, the dashed green line is the speed bias (AMV-rawinsonde) profile, and the red curve is the mean rawinsonde speed profile.**

Layer of Best Fit Analysis

The objective of this analysis is to further evaluate the concept that an AMV better corresponds to a layer of the atmosphere rather than flow at any single level. The results shown here involve comparisons between NOAA/NESDIS operational GOES-12 AMVs and rawinsondes launched at the ARM SGP Central Facility for a 1 year period (April 2005-2006). ARM sonde data has a time resolution of 2 seconds, providing a large number of wind observations at a very high vertical resolution, which are essential for this type of analysis. For the layer best fit analysis, an AMV is compared with layer-averaged sonde data, with layer depths increasing from 20 to 400 hPa. A "level of best fit" analysis is also performed in conjunction with this layer analysis. For this level analysis, an AMV is compared to the entire depth of a sonde wind profile, and the level with the minimum AMV-sonde vector difference is found.

A summary of these results is shown in Figure 12. The curves show AMV to layer-averaged rawinsonde vector RMS differences for GOES-12 6.7 μm WV and 10.7 μm IR window channel vectors of varying height layers. Plotted on the y-axis are the level of best fit vector RMS values, corresponding to the channel and height of vectors from the colored curves. The results show that upper-level IR and WV AMVs best correspond to a 100 hPa thick layer. For low to mid-level IR AMVs, the layer of best fit increases to a ~150 hPa thickness. Mid-level (presumably clear-sky) WV AMVs do not show a clear layer-mean signal. The AMV-sonde vector RMS at the layer of best fit for all AMV

types except low-level IR show improvement over the VRMS found at the level of best fit. This suggests that, in most situations, AMVs correspond better with a layer-mean flow than that from any single level height assignment.

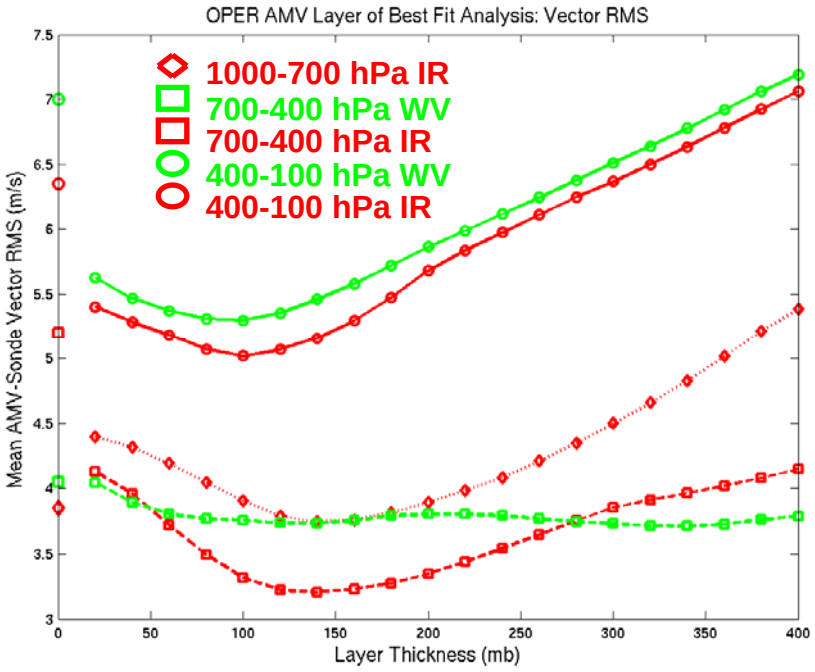

Figure 12. **A comparison between layer averaged rawinsonde data and NOAA/NESDIS operational GOES-12 AMVs for various satellite channels and heights. Plotted on the y-axis are vector RMS values found at the level of best fit for the vectors included in the colored curves.**

3.7 Attempts to Improve GOES Image Navigation

In this research we analyze the impact of various navigation parameter errors on image navigation accuracy. Methods that employ the Earth edge and image center are tested for GOES imagery. Navigation that is based on earth center determination from earth edge measurements does not rely on landmarks and hence is not vulnerable to excessive cloud cover. Navigation performance within one pixel has been realized at the Chinese National Satellite Meteorological Center for their spinning FY2B. An image center time series analysis indicates that, for the three axis stabilized GOES-9 during the Western Pacific observation mission, the image navigation accuracy is significantly reduced by errors in the forecast of spacecraft attitude. The biases in the roll and pitch can be nearly eliminated by introducing the attitude signal derived directly from earth center information.

Image navigation is an essential and fundamental component in data processing of geosynchronous meteorological satellite. It is based on S/C attitude, misalignment and orbit parameters. Image navigation parameters are derived from landmarks, star sensing and ranging. Navigation performance within one pixel has been realized at the Chinese National Satellite Meteorological Center for their spinning FY2B, which did not depend on any landmark matching, but just by deriving image navigation parameters from image center time series. GOES I-M are first in the series of 3-axis stabilized geosynchronous meteorological satellites. However, this makes image navigation parameter solutions and forecasting more complex. The S/C in-flight attitude bias, thermal distortions and earth sensors bias will decrease image navigation accuracy.

Here we introduce a new GOES image navigation method, based on the technique developed for Chinese FY2 satellite. It corrects image navigation parameters independent of landmarks, using image center (nadir) and image Morphologic information. An R&D system was developed to verify the new image navigation method. Figure 13 shows how it works. According to the simulation and bias

analysis, different navigation parameters have different effects on image navigation; the most important part is S/C attitude. The Green zone in the flowchart has been finished, correcting S/C roll and pitch parameters automatically. The Red zone in the flowchart needs imager star sensing information that we can't access at present. Therefore, an interactive operation is employed to correct S/C Yaw; this part in the flowchart is marked in yellow.

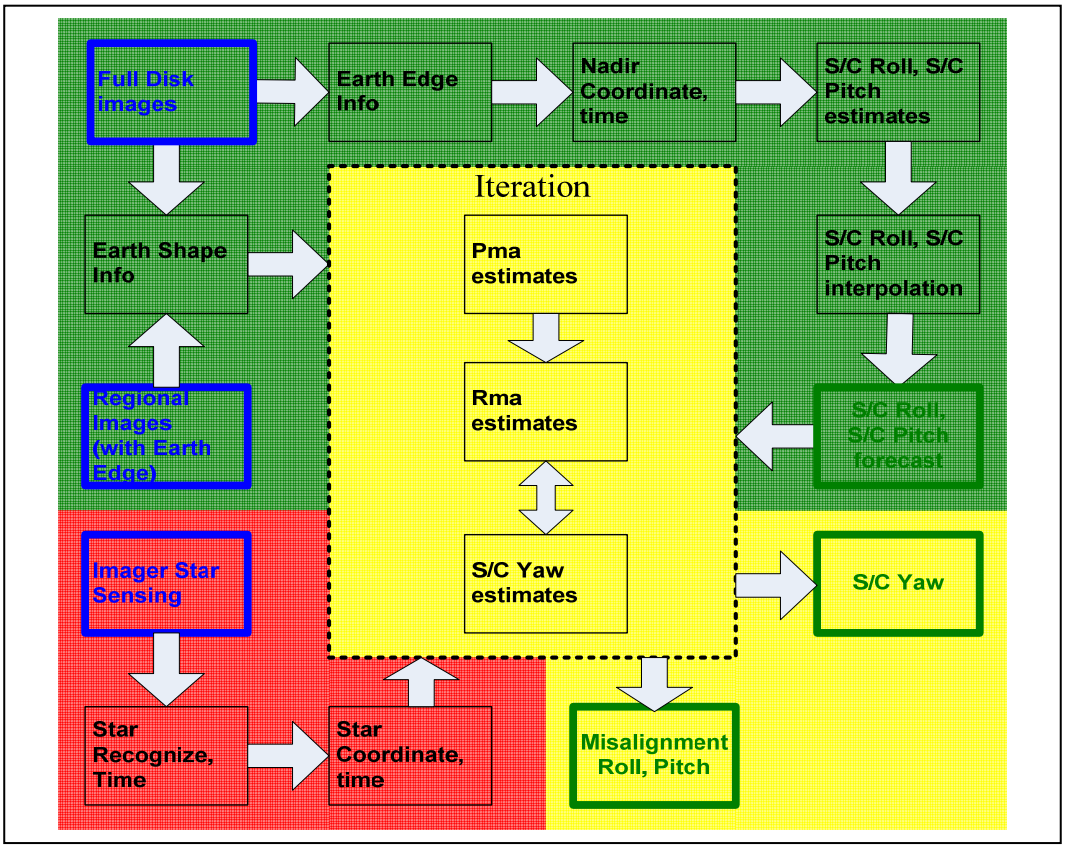

Figure 13. **Improved Image Navigation Parameter Decision Flowchart**

Experiments involving the effects of the proposed navigation method on AMV validation are given. The first test involved correcting the S/C roll and pitch parameters automatically. The second test used an interactive S/C yaw correction. Both tests renew the image navigation parameters, write them back to dataset files, and these values were then used in CIMSS's AMV retrieval system to derive AMV and assess validations.

A homogeneous comparison of AMVs with collocated raobs is presented in Table 3. As shown, the AMVs are improved just using the automatic correction of S/C roll and pitch parameters, and improved slightly over the current CIMSS landmark navigation based AMVs. The important finding of this new method is that it could apply for cases lacking in landmarks, and could be used for attitude forecast and applied to regional scans like SRSO or RSO. Combined with imager star sensing data, it would be possible build up a complete automatic image navigation system; the Interactive Image Navigation test demonstrated this possibility. The current test was based on GOES 9, which operates on IMC "OFF" mode. For GOES 10/12 working in the IMC "ON" mode, the new method would need some slight modification

	CIMSS Landmark Navigated	**S/C Roll, Pitch Auto corrected**	**S/C Roll, S/C Roll, Pitch corrected S/C Yaw, PMA and RMA**

					interactive corrected	
AMV Tracing Method	**RAW**	**AQC**	**RAW**	**AQC**	**RAW**	**AQC**
Matching Distance	**100Km**	**100Km**	**100Km**	**100Km**	**100Km**	**100Km**
Homogeneous Comparisons						
Samples	**246**	**113**	**246**	**113**	**246**	**113**
Speed Bias	**0.51**	**2.15**	**-0.03**	**1.59**	**-0.08**	**1.27**
VRMS	**8.73**	**6.29**	**8.64**	**5.70**	**8.53**	**5.51**
Average Vector Relocation Distance (Km)						
Match with Uncorrected Images	**3.21**	**5.45**	**26.64**	**26.34**	**27.16**	**26.62**

Table 3. **Image Navigation Validation: Effect on AMVs**

3.8 Wind Vector Calculations Using Simulated Hyperspectral Satellite Retrievals

Image triplets of constant pressure level moisture analyses calculated from simulated hyperspectral satellite retrievals are examined for possible wind vector tracking. This method adapts the existing automated wind tracking code used operationally at NOAA/NESDIS. The modified code eliminates the necessity of the computationally expensive height assignment algorithms, as the altitude of the moisture surfaces being tracked is provided by the retrieval output. The moisture retrievals are analyzed at 101 pressure levels, and simulate the Geostationary Imaging Fourier Transform Spectrometer (GIFTS), the Hyperspectral Environmental Suite (HES), and the Atmospheric Infrared Sounder (AIRS) processing. From a selection of these levels, winds can be derived in clear sky by tracking the advecting moisture features in the image triplet. As a result, vertical profiles of winds can be produced.

In preparation for the launch of the GOES-R mission, CIMSS is working on a risk reduction program. Algorithm development, data processing, archiving, data assimilation, nowcasting and outreach are activities being researched. The risk reduction program will hopefully produce a set of products that can be applied to the future hyperspectral imagers and sounders to be launched in the next decade. Winds development is a subset of the algorithm development element.

Several steps are involved in producing the clear sky profiles of winds. Mesoscale models are used to generate simulated atmospheric profiles with detailed horizontal and vertical resolution. Top of atmosphere (TOA) radiances are determined using these profiles along with the GIFTS forward radiative transfer model. Single field of view temperature and water vapor retrievals are calculated from the TOA radiances. Targets and clear-sky AMVs derived from constant pressure water vapor analyses are produced.

Atmospheric temperature and water vapor profiles will be one of the primary products to be retrieved from GIFTS or HES. The water vapor profiles are used as data input into the AMV calculations. The current retrieval algorithms for GIFTS and HES were born from aircraft instruments such as the High resolution Interferometer Sounder (HIS), NPOESS Airborne Sounder Testbed Interferometer (NASTI) and from the existing space based Atmospheric Infrared Sounder (AIRS). The full method utilizes a statistical retrieval followed by a nonlinear iterative physical retrieval solution. It is too computationally expensive to perform both methods in our simulations, so the statistical regression algorithm output is used as input into the AMV software.

The AMV algorithm takes the retrieved moisture analyses, at constant pressure levels, and converts them into an image for the CIMSS AMV algorithm. The water vapor amount is stretched over a range of 0 to 255 brightness counts in these images. Clouds are masked, and not used in this process. This has also been done for WRF model mixing ratios, used in comparisons. A sequence of three images

(30 minutes to an hour apart) is animated and features are targeted and tracked. The height of the AMV is pre-determined by the retrieval output. Height assignment errors that afflict current wind production should be minimized. The hyperspectral information (retrievals at 101 pressure levels) allows AMV production at multiple vertical levels.

A WRF model simulation was initialized at 0000 UTC, 24 June 2003, and run for 30 hours. 30-minute data was available from this simulation. 101 pressure levels were available for each time period. Winds were calculated in between. Figure 14 shows the vertical wind density from 683mb down to 986mb at every available pressure level achieved in this simulation.

The results demonstrated here clearly illustrate the concept. More work remains and will continue to be done in the future.

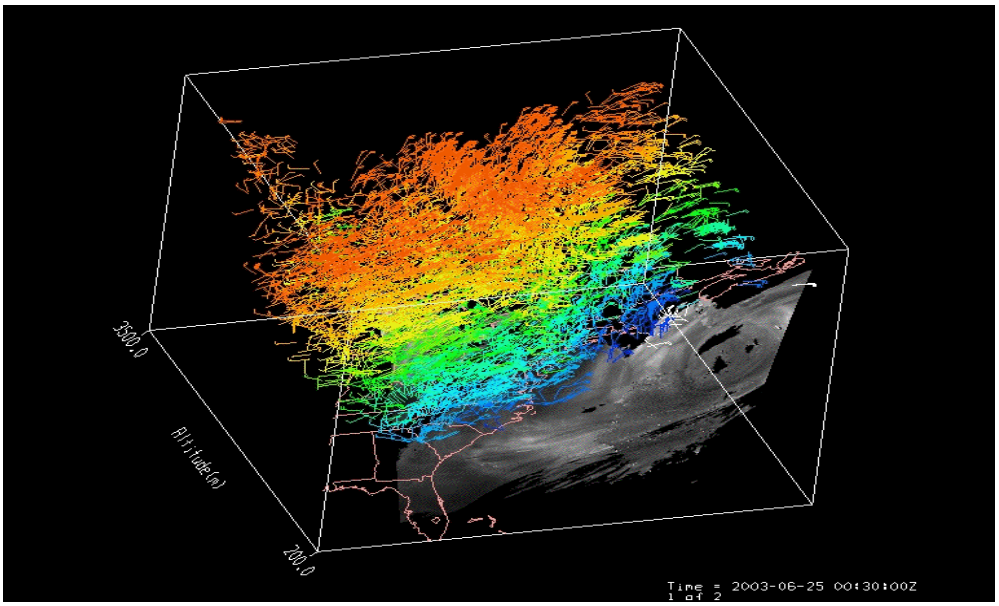

Figure 14. **IDV display of clear-sky WV AMVs derived from simulated hyperspectral moisture retrievals.**

3.9 Satellite Wind Vectors from GOES Sounder Moisture Fields

GOES-East and GOES-West sounders provide real-time retrievals of temperature and moisture in cloud-free regions on an hourly basis. In November 2005, NOAA/NESDIS implemented a new integrated GOES sounder product processing system that derives atmospheric products such as clear sky radiances, temperature and moisture profiles, cloud-top pressure and surface skin temperature at the full GOES sounder resolution of about 10km^2. These products have not only better geographical coverage, but also provide improved depiction of gradient information, which allow for constant pressure level moisture analysis fields of significant contrast to be extracted and used as input to a wind retrieval algorithm. The vertical profiles can be converted to images at all or selected pressure levels that then serve as input image sequences for satellite wind retrieval algorithms. By their nature, the sounder generated moisture fields will overcome the problem of determining heights of the wind vectors. This work is an attempt to deduce winds from dew point temperature (*Td*) images with the current feature tracking CIMSS satellite-derived wind algorithm producing wind fields every 3 hours.

Preliminary results from deriving satellite wind vectors from GOES sounder dew point temperature (*Td*) fields for 5 December 2003 are shown in Figure 15 which illustrates the horizontal and vertical distribution of these AMVs. Again, these results prove the feasibility of the approach.

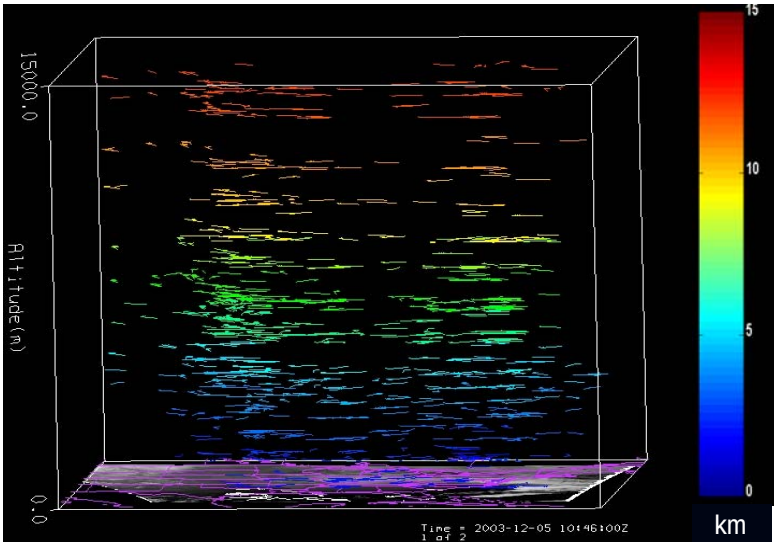

(a)

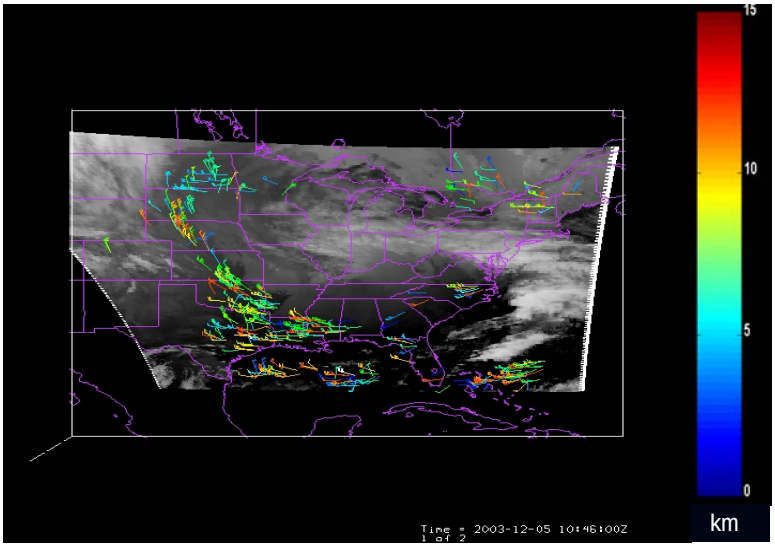

(b)

Figure 15. **Vertical** (top) **and horizontal** (bottom) **distribution of clear-sky WV AMVS derived from the GOES sounder derived product dew point temperature fields (bottom).**

Additional research aimed at improving the GOES sounder moisture winds will address the following topics: improving the image extraction scheme; applying dynamic search box size with altitude; extracting mixing ratio fields; further algorithm verification with RAOBs and wind profiling radar data; implementing the approach in real time; producing long term statistics; and initiating data assimilation efforts.

Acknowledgments

Steve Wanzong, Iliana Genkova, Howard Berger, Kristpher Bedka, and Feng Lu from CIMSS are thanked for their contibutions to this report.

References

Barron, J.l, D.J Fleet, and S.S. Beauchemin, 1994: Systems and Experiments; Performance of Optical Flow Techniques. *International Journal of Computer Vision*, 12:1, 43-77.

LeMarshall, J. A., A. Rea, L. Leslie, R. Seecamp, and M. Dunn, 2004: Error characterization of atmospheric motion vectors. *Aust. Meteor. Mag.*, 53, 123-131.

Lucas, B. and T. Kanade, 1981: An iterative registration technique with an application to stereo vision. *Proc. 7th Int. Joint Conf on Artificial Intelligence*, Aug 24-28, Vancouver, British Columbia, 674-679.

Santek, D., J. Key, C. Velden, and N. Bornemann, 2002: Deriving winds from polar orbiting satellite data. *Proc. Sixth Int. Winds Workshop*, Madison, Wisconsin, EUMETSAT, 251-261.

Sonka, M., Hlavac, V. and R. Boyle, 1993: *Image Processing, Analysis and Computer Vision*, Chapman and Hall Computing.